

Fuzzy PID Controller Optimized by Improved Gravitational Search Algorithm for Load Frequency Control in Multi-area Power System

Gonggui Chen, Feng Qin, Hongyu Long*, Xianjun Zeng, Peng Kang, and Jinming Zhang

Abstract—In this paper, an objective function considering performance index and an improved gravitational search algorithm (IGSA) are proposed to optimize the parameters of fuzzy PID (FPID) controller. IGSA is obtained by combining elite strategies and the mining capability of PSO algorithm. The IGSA FPID method which integrates IGSA and FPID controller is tested in a typical two-area non-reheat system, and system responses reflect the advantages of proposed objective function and IGSA. Additionally, the proposed IGSA FPID method still has excellent effects even on the two-area multi-source system with thermal power, hydropower and gas turbines. Meanwhile, the effect of high voltage direct current (HVDC) links in suppressing fluctuations is verified. Due to the popularity of wind power, a novel three-area interconnected power system with nonlinearity connected wind turbine (WT) is designed. Under the control of IGSA FPID, the good stability and dynamic performance of mentioned three-area system are verified. Therefore, FPID controller optimized by IGSA has excellent control effects, stability and universal applicability on the different power systems with multiple area and sources.

Index Terms—Load Frequency Control, Fuzzy PID Improved Gravitational Search Algorithm, Multi-source, Wind turbine.

I. INTRODUCTION

IN the interconnected power system, load frequency control (LFC) is the focus and difficulty of power systems. It is also an important guarantee for maintaining the stable operation of systems [1]. With the expansion of power systems and the increase in electric demand, the style of power generation has

gradually developed from single source to multi-source, which results in more complex frequency changes. Additionally, wind power is promoted because of its cleanliness, so it is a trend that wind power is connected to power grids. Wind power is uncertain, which makes LFC more difficult. Therefore, a control strategy with fast response and strong stability is urgently needed.

The main goal of LFC is to maintain balance between power generation and load demand, and then minimize the deviation of frequency and tie-line power under load disturbances. To some extent, LFC determines whether the power system runs normally. The selection and design of controller largely affects stability and dynamic performance of LFC. In recent years, many control strategies have been proposed. Proportional integral derivative (PID) controller was first proposed and has been widely used in research and practical engineering, because it has simple but reliable structure [2]. Regarding tuning the parameters of PID controller, some intelligent algorithms are proposed. Backtracking search algorithm is adopted to solve LFC problem [3]. Moreover, quite a few algorithms such as BFOA [4], PSO [5] and IFABC [6] are proposed to search for optimal parameters. On the basis of PID controller, many new PID controllers have been developed, such as adaptive PID [7], fractional order PID [8], robust PID [9] and FPID. Meanwhile, many strategies except PID were presented. Yang et al. [10] introduced model predictive control for LFC in hybrid power system. A scheme named dual loop-internal model control is proposed for the LFC of multi-area multi-sources power systems [11]. Mi et al. [12] employed sliding mode load frequency control for hybrid power system.

Among those control strategies, FPID is one of the most popular methods in current research. It perfectly inherits the advantages of PID, and solves the problem that the performance and stability of PID are degraded in nonlinear power system. Many documents proposed different strategies to optimize FPID. For example, Chen et al. [13] search for optimal parameters by improved ant colony optimization algorithm. Simulation results of those literatures also prove that FPID can meet higher goals and requirements, what's more, it can be deeply explored.

The model of the power system is another important aspect. With the deepening of research, models have gradually evolved from basic two-area non-reheat model to multi-area multi-source and they are more practical. Sahu et al. [14] and Mishra et al. [15] designed different two-area multi-source interconnected power system. Three-area hydro-thermal

Manuscript received June 23, 2021; revised November 27, 2021. This work was supported by the National Natural Science Foundation of China under Grant 51207064.

Gonggui Chen is a professor of Key Laboratory of Industrial Internet of Things and Networked Control, Ministry of Education, Chongqing University of Posts and Telecommunications, Chongqing 400065, China; (e-mail: chengpower@126.com).

Feng Qin is a graduate student of Chongqing University of Posts and Telecommunications, Chongqing 400065, China (e-mail: cquptqf@163.com).

Hongyu Long is a professor level senior engineer of Chongqing Key Laboratory of Complex Systems and Bionic Control, Chongqing University of Posts and Telecommunications, Chongqing 400065, China (corresponding author to provide phone: +8613996108500; e-mail: longhongyu20@163.com).

Xianjun Zeng is a senior engineer of State Grid Chongqing Electric Power Company, Chongqing 400015, China (e-mail: 13594255525@139.com).

Peng Kang is a senior engineer of Economic and Technology Research Institute, State Grid Chongqing Electric Power Company, Chongqing 401120, China (e-mail: 1060846892@qq.com).

Jinming Zhang is a senior engineer of State Grid Chongqing Electric Power Company, Chongqing 400015, China (e-mail: zjm213@163.com).

system and three-area nonlinear system with time delay, generation rate constraint (GRC) and governor dead band (GDB) are proposed in [16]. Furthermore, the four-area unequal power system connected reheat, WT and photovoltaic (PV) is also designed [17]. Those existing strategies have realized stable control. In order to explore new strategies to obtain better results, GSA is improved to promote the capability of optimization. The main contributions of this paper are as follows.

(i) A novel three-area unequal power system is designed, in which nonlinearities such as GDB and GRC are considered, and WT is connected into the system. Besides, IGSA FPID has a good ability to control this system.

(ii) By introducing the elite strategy and combining the mining capability of PSO, an improved GSA is proposed to search for the optimal parameters of FPID.

(iii) A new function combining existing objective function and performance index is designed, which considers undershoot (*US*), overshoot (*OS*) and setting time (*T_s*), and introduces a penalty coefficient *F* determined by steady state error (*Ess*).

Furthermore, a random load considering intermittent-large and continuous-small disturbances is designed, and the influence of HVDC on frequency and tie-line power is explored.

II. SYSTEM METHODOLOGY

A. LFC model

Modern power grids are mostly interconnected power systems by tie-line, so it is necessary to consider not only the balance between generation and load demand in local area but also the power change on tie-line. According to the deviation of frequency and tie-line power, controllers adjust governors to reduce area control error (*ACE*). *ACE* can be expressed by (1). When *ACE* is reduced to 0, all deviations drop to 0.

$$\begin{cases} ACE_1 = B_1 \Delta f_1 + \Delta P_{tie} \\ ACE_2 = B_2 \Delta f_2 + a_{12} \Delta P_{tie} \end{cases} \quad (1)$$

where Δf_1 and Δf_2 are incremental change of frequency in area-1 and area-2, and ΔP_{tie} is tie-line power deviation.

A typical two-area no-reheat system consists of controllers, governors, turbines, power systems and tie-line. The model shown in Fig.1 [13] was widely used in documents about LFC, so it can verify the performance of controller by compared with the system response of those controller which used same model.

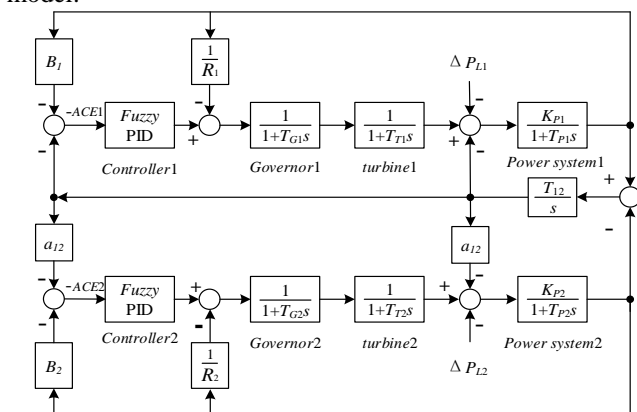


Fig.1 Two-area non-reheat power system

In this model, a_{12} is the balance coefficient of tie-line power, B is the frequency deviation factor, R is the governor speed regulation parameter, T_G is the governor time constant, T_T is the turbine time constant, T_P is the synchronizing coefficient, T_P is the time constant of connected power system and K_P is the gain of connected power system.

B. Fuzzy PID controller

Fuzzy PID is a control theory combining PID and fuzzy control. A famous professor of California University, L.A. Zaden, first proposed concept of fuzzy control in 1990s. Fuzzy control is suitable for complex systems with time delay and nonlinearity because of its excellent robustness, but it has poor performance in eliminating *Ess*. PID is simple, reliable and easy to adjust, but it does not work well for nonlinear or inaccurate systems. Fuzzy PID combines strengths of fuzzy control and PID, so it is widely researched and designed by many scholars.

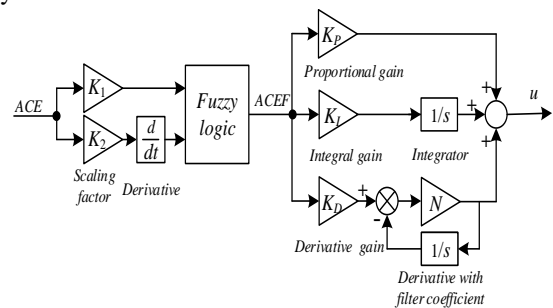


Fig.2 Structure of fuzzy PID Controller

Fuzzy PID control [18, 19] is a control theory combining PID and fuzzy control (FC). A famous professor of California University, L.A. Zaden, first proposed concept of fuzzy control in 1990s. Fuzzy control is suitable for complex systems with time delay and nonlinearity because of its excellent robustness, but it has poor performance in eliminating *Ess*. Fuzzy PID combines strengths of fuzzy control and PID, so it is widely used in industrial production.

The structure of fuzzy PID is shown in Fig.2, and it can be divided into fuzzy logic and PID. Fuzzy logic mainly consists of fuzzy inference system (FIS), membership function (MF) and fuzzy rule (FR). FIS implements main settings and operations of fuzzy logic, and the whole process of calculation is as follows. FIS fuzzifies input according to MF, and then converts fuzzy input into fuzzy output by fuzzy logic table, finally, FIS defuzzifies fuzzy output to get accurate output. Therefore, fuzzy logic knows error and its changing trend according to *ACE* and *ACE* deviation, and then new *ACE* (*ACEF*) is obtained.

MF is usually three-dimension, five-dimension or seven-dimension, and each dimension is average. However, three-dimensional MF cannot achieve sufficient effects, and there are too many FR in seven-dimensional MF, which leads to long running time. Because *ACE* and *ACE* deviation are small signals, a five-dimensional MF is adopted. These dimensions are mainly concentrated near 0, so that MF has a better ability to distinguish and process when facing small *ACE*. MF is shown in Fig.3, and five dimensions are separately negative big (NB), negative small (NS), zero (Z), positive small (PS) and positive big (PB). TABLE I shows the rule of fuzzy logic in this paper[13], and the method of

defuzzification is named centroid. Centroid means that the gravity of the area enclosed by MF and abscissa is regarded as the final output of fuzzy logic.

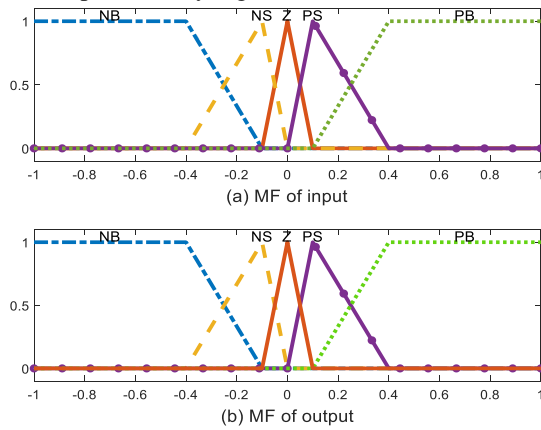


Fig.3 MF of fuzzy logic

TABLE I
FUZZY LOGIC TABLE

$\frac{d(ACE)/dt}{ACE}$	NB	NS	Z	PS	PB
NB	NB	NB	NS	NS	Z
NS	NB	NS	NS	Z	PS
Z	NS	NS	Z	PS	PS
PS	NS	Z	PS	PS	PB
PB	Z	PS	PS	PB	PB

Regarding PID controller, the PID with filter coefficient is adopted in this article. When controlled system has fluctuations and noise, a suitable filter coefficient can smooth the input signal, and improve the performance of PID. The output u can be calculated and corresponding equation can be expressed by (2)

$$u = ACEF \cdot \left(K_p + K_I \frac{1}{s} + K_D \frac{N}{1 + N/s} \right) \quad (2)$$

Some parameters in Fig.2 require being explained. K_1 and K_2 are scaling factor of ACE and ACE derivative, K_p , K_I and K_D are gain of PID, N is the filter coefficient. Those parameters directly affect dynamic performance of controller. In order to make fuzzy PID have better performance, GSA is improved and adopted to optimize parameters of fuzzy PID.

C. Main objective functions

Objective functions can simulate environmental effect and select some individuals with good performance. Algorithms can update the whole population according to those selected individuals, and finally achieve the goal of optimization. In this paper, the relevant parameters of individuals are imported into designed LFC model, and individual fitness is calculated by objective functions. Four methods [20] as follows are mainly adopted.

(i) Integral of Time multiplied Absolute Error (ITAE)

$$ITAE = \int_0^{t_{sim}} t \cdot (|\Delta f_1| + |\Delta f_2| + |P_{tie}|) dt \quad (3)$$

(ii) Integral of Time multiplied Squared Error (ITSE)

$$ITSE = \int_0^{t_{sim}} t \cdot (|\Delta f_1| + |\Delta f_2| + |P_{tie}|)^2 dt \quad (4)$$

(iii) Integral of Absolute Error (IAE)

$$IAE = \int_0^{t_{sim}} (|\Delta f_1| + |\Delta f_2| + |P_{tie}|) dt \quad (5)$$

(iv) Integral of Squared Error (ISE)

$$ISE = \int_0^{t_{sim}} (|\Delta f_1| + |\Delta f_2| + |P_{tie}|)^2 dt \quad (6)$$

All main objective functions are integral calculations of errors, and they did not consider the influence of other factors. However, there is a problem in main objective functions. When these functions are used to search for smaller value, a larger US or OS may occur, which seriously affects the stability of controlled system. In order to obtain better response and performance index of controlled system, it's necessary to design an objective function which has better performance of evaluation. Under the foundation of the objective function with excellent performance, a new objective function is proposed which considering US , OS and T_s , and introducing the penalty coefficient F determined by Ess . US , OS and T_s will be multiplied by their corresponding weights, and the role of the weight is to ensure the value of each part in the new function is similar. What's more, weights are adjusted to fit controller and controlled system. The equation of new objective function is mentioned later.

D. Improved Gravitational Search Algorithm

A new heuristic algorithm named gravitational search algorithm [21] was proposed in 2009. It is derived from the law of universal gravitation and Newton second law and searches for optimal solution by gravitational force [22] between individuals. The individual with better performance has higher mass and stronger gravitational force. With the iteration of algorithm, individuals rely on gravitational force to move continuously in search space. Finally, individuals find the optimal position, which means that the optimal solution is found. The interaction of gravitation does not need any medium, so each individual in searching space can obtain information of global environment.

It is assumed that there are P individuals in D -dimensional space, so gravitational force between the i -th individual and the j -th one is (7).

$$F_{ij}^d(t) = G(t) \frac{M_i(t)M_j(t)}{\|X_i(t), X_j(t)\|_2} (x_j^d(t) - x_i^d(t)) \quad (7)$$

where $G(t)$ is gravitational constant, M_i and M_j are the i -th and the j -th individual mass, X_i and X_j are the i -th and the j -th individual position.

Each individual mass is defined by its fitness according to (8), and fitness is calculated by the selected objective function.

$$m_i = (f_i - f_{worst}) / (f_{best} - f_{worst}) \quad (8)$$

where f_i is the i -th individual fitness, f_{worst} is the worst individual fitness, f_{best} is the best individual fitness, m_i is usually normalized by (9).

$$M_i = m_i / \sum_{j=1}^N m_j \quad (9)$$

Every individual is affected by from other individuals, so the total force can be represented by a random and weighted sum of all gravitational forces. The equation of total force is described by (10).

$$F_i^d(t) = \sum_{j=1, j \neq i}^N rand \cdot F_{ij}^d(t) \quad (10)$$

Acceleration a is calculated by Newton second law, so velocity v and position x are updated by (11).

$$\begin{aligned} v_i^d(t+1) &= r \cdot v_i^d(t) + a_i^d(t) \\ x_i^d(t+1) &= x_i^d(t) + v_i^d(t+1) \end{aligned} \quad (11)$$

where v_i^d and a_i^d are respectively the i -th individual velocity and acceleration, r is random number in $[0, 1]$.

Original GSA can also optimize the parameters of controller, but it has some defects. Firstly, in original GSA, all individuals participate in the updating of gravitational force. Some individuals with poor performance may make results worse and slow the speed of iteration. Secondly, it only relies on acceleration to update the speed and position, which is easy to fall into local optimization. To solve the shortcomings of original GSA, two improvements are proposed, and whole flowchart of IGSA is shown in Fig.4.

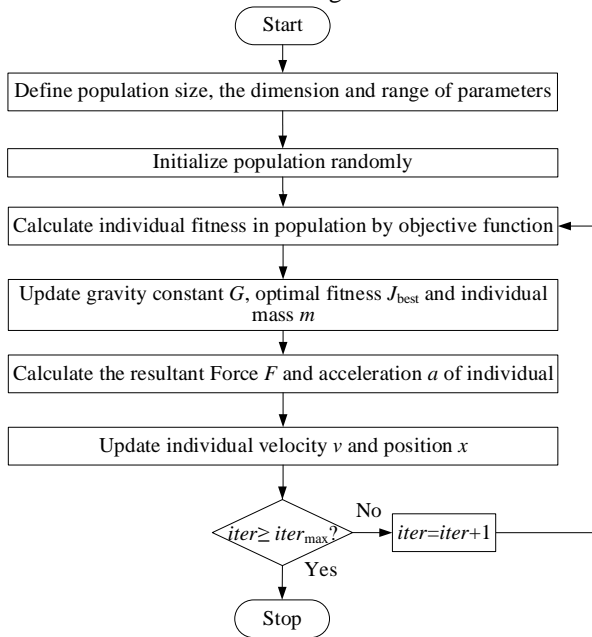


Fig.4 Flowchart of IGSA

The detailed improvement measures are as follows.

(i) Elite strategy

Elite strategy is that some individuals with better performance are selected to update resultant and acceleration, so as to avoid decreasing accuracy due to poorly performing individuals participate. When the number of iterations increases, the number of elites decreases. This modification can continuously update the number of elites and make the result under the influence of elites closer to the optimal results. The number of elites is determined by (12).

$$num = \text{round}(num_{last} + P \cdot (1 - t/T) \cdot (1 - num_{last}/100)) \quad (12)$$

where num is number of elites, P is number of population, t and T are respectively number of current iteration and max iteration, $num_{last} = 2$, which ensures at least two individuals that participate in update.

(ii) Combining the mining capability of PSO

For better capability about global search, combining characteristics of PSO, the ability of social information exchange is added in GSA, so (13) is updated equation of velocity.

$$\begin{aligned} v_i^d(t+1) &= r_1 \cdot v_i^d(t) + a_i^d(t) + c_1 \cdot r_2 \cdot (p_{best}^d - x_i^d) \\ &+ c_2 \cdot r_3 \cdot (g_{best}^d - x_i^d) \end{aligned} \quad (13)$$

where r_1 , r_2 are random number in $[0, 1]$, c_1 , c_2 are learning factors, p_{best} and g_{best} are local and global optimal position.

By adjusting c_1 and c_2 , the influence of social information exchange can be adjusted during individual movement. IGSA needs sufficient ability about global search to avoid falling into local optimum in early period, but in later period of iteration, strong ability about local search is needed to improve accuracy, so c_1 and c_2 are updated by(14).

$$c_1 = 2(1 - e^{-G_0(\frac{t}{T})^2}), \quad c_2 = 2e^{-G_0(\frac{t}{T})^2} \quad (14)$$

where G_0 is original gravitational constant.

III. RESULTS AND DISCUSSION

The simulation of following designs were conducted on an Intel Core i5-7500 CPU of 3.4 GHz and 12 GB RAM computer in MATLAB (R2016a) environment.

A. Standard functions

In order to prove that those improvements of the algorithm are effective, six standard functions shown in TABLE II are used. Dimension D is 100, population P is 50, the number of iterations is 2000, and algorithm runs 30 times repeatedly.

TABLE II
SIX STANDARD FUNCTIONS

Function name	Function equation	Range
Sphere (f_1)	$f_1(x) = \sum_{i=1}^D x_i^2$	$[-100, 100]^D$
Schwefel (f_2)	$f_2(x) = \sum_{i=1}^D x_i + \prod_{i=1}^D x_i $	$[-10, 10]^D$
Rosenbrock (f_3)	$f_3(x) = \sum_{i=1}^{D-1} [100(x_{i+1} - x_i^2)^2 + (x_i - 1)^2]$	$[-10, 10]^D$
Rastrigin (f_4)	$f_4(x) = \sum_{i=1}^D [x_i^2 - 10 \cos(2\pi x_i) + 10]$	$[-5.2, 5.2]^D$
Ackley (f_5)	$f_5(x) = -20 \exp(-0.2 \sqrt{D^{-1} \sum_{i=1}^D x_i^2}) - \exp(D^{-1} \sum_{i=1}^D \cos 2\pi x_i) + 20 + e$	$[-32, 32]^D$
Griewank (f_6)	$f_6(x) = \frac{1}{4000} \sum_{i=1}^D x_i^2 - \prod_{i=1}^D \cos(\frac{x_i}{\sqrt{i}}) + 1$	$[-600, 600]^D$

TABLE III
THE RESULTS OF SIX STANDARD FUNCTIONS

F		PSO	ABC	GSA	IGSA
f_1	MEAN	3.72×10^{-5}	3.99×10^{-4}	1.69×10^{-16}	8.09×10^{-17}
	STDEV	1.28×10^{-4}	1.13×10^{-4}	1.88×10^{-19}	1.10×10^{-18}
	BEST	8.39×10^{-9}	1.46×10^{-4}	1.26×10^{-16}	2.79×10^{-17}
	WORST	7.01×10^{-4}	6.55×10^{-4}	2.33×10^{-16}	1.92×10^{-16}
f_2	MEAN	5.44×10^1	8.05×10^1	4.62×10^{-8}	4.53×10^{-8}
	STDEV	1.78×10^1	1.45×10^1	1.06×10^{-9}	2.88×10^{-9}
	BEST	2.00×10^1	5.12×10^1	3.99×10^{-8}	2.95×10^{-8}
	WORST	1.00×10^2	1.23×10^2	5.53×10^{-8}	7.02×10^{-8}
f_3	MEAN	1.15×10^4	1.81×10^3	8.13×10^{-4}	1.59×10^{-4}
	STDEV	3.52×10^3	2.07×10^2	8.29×10^{-4}	1.47×10^{-4}
	BEST	7.88×10^3	1.47×10^3	4.65×10^{-5}	1.76×10^{-5}
	WORST	1.51×10^4	2.02×10^3	2.15×10^{-3}	3.80×10^{-4}
f_4	MEAN	4.74×10^2	1.55×10^2	7.39×10^1	1.14×10^1
	STDEV	5.47×10^1	1.59×10^1	8.59×10^1	3.08×10^0
	BEST	3.94×10^2	1.30×10^2	5.67×10^1	5.97×10^0
	WORST	5.98×10^2	1.76×10^2	8.86×10^1	1.69×10^1
f_5	MEAN	1.21×10^1	4.22×10^{-3}	8.65×10^{-9}	7.04×10^{-9}
	STDEV	8.68×10^0	7.99×10^{-4}	1.06×10^{-10}	2.68×10^{-11}
	BEST	4.08×10^{-5}	2.94×10^{-3}	6.51×10^{-9}	4.40×10^{-9}
	WORST	2.00×10^1	6.17×10^{-3}	1.08×10^{-8}	9.86×10^{-9}
f_6	MEAN	3.44×10^1	1.98×10^1	2.92×10^{-1}	5.49×10^{-2}
	STDEV	1.09×10^1	1.21×10^1	6.19×10^{-1}	1.31×10^{-1}
	BEST	2.14×10^1	4.19×10^0	9.26×10^{-2}	1.72×10^{-2}
	WORST	5.90×10^1	3.76×10^1	1.55×10^1	3.37×10^{-1}

TABLE III shows the results of the mean, standard deviation, best, and worst respectively. The results in TABLE III show that all best indicators are obtained by GSA or IGSA. When dealing with simple problems (such as f_1), the results of PSO and ABC are 10^{-4} , but GSA is 10^{-16} . When facing complex problems, although the accuracy of GSA decreases, it still has the best performance. In addition, except for a small number of indicators, other indicators of IGSA are better than GSA. Those results prove that GSA has stronger ability of optimization than PSO, ABC, and these improvements make GSA have a great promotion.

B. Two-area non-reheat power system

The model is shown in Fig.1, and detailed parameters are listed in Appendix A. According to some existing literatures, the parameters of IGSA and the range of controller parameters are set as follows. Population P is 50, iteration is 100 and original gravitational constant G_0 is 30 [16]. K_1 , K_2 , K_P , K_I and K_D belong to $[0, 2]$ [13], and N belongs to $[0, 200]$.

The best one of 20 simulation results is chosen as parameters of FPID. Under the condition of 10% load disturbance in area-1, the performance of GSA and IGSA was tested. Iteration curves are shown in Fig.5, and relevant data are in TABLE IV. IGSA effectively avoided falling into local

optimum and improved the accuracy of results, which proves IGSA has better ability in search and optimization.

The parameters of IGSA FPID are optimized by main objective functions. ITSE has the best performance and it is selected to construct new function J as shown in (15).

$$J = F \cdot (ITSE + \omega_1 \cdot Ts + \omega_2 \cdot |US| + \omega_3 \cdot |OS|) \quad (15)$$

where ω is weight of each part, Ts is the sum of all setting time. $|US|$ is the sum of all absolute value of undershoot, $|OS|$ is the sum of all absolute value of overshoot, F is the penalty coefficient which determined by the Ess according to (16).

$$F = \begin{cases} 1 & \text{if } |Ess| < 10^{-5} \\ 10000 & \text{if } |Ess| > 10^{-5} \end{cases} \quad (16)$$

In this model, $\omega_1=0.005$, $\omega_2=0.6$, $\omega_3=10$. After J is used to optimize parameters, the system responses under different objective functions are shown in Fig.6. Results show that with the help of J , US is significantly decreased, and its value is only 60% of other objective functions. What's more, other performance indicators are also improved to some extent. The result in Fig.7 show responses of controlled system when the algorithm or the objective function is improved, which proves the effectiveness of modification both in algorithm and in objective function.

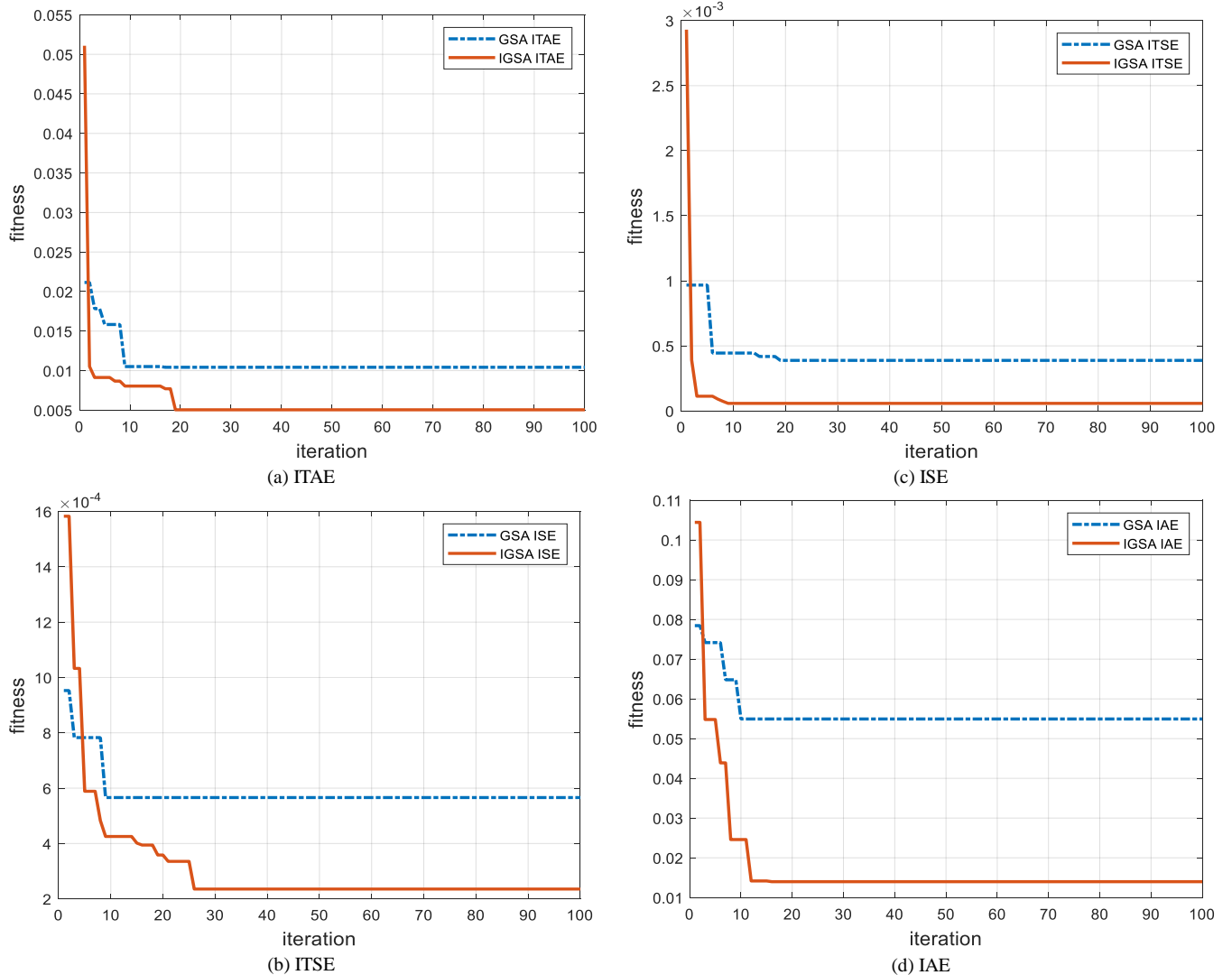


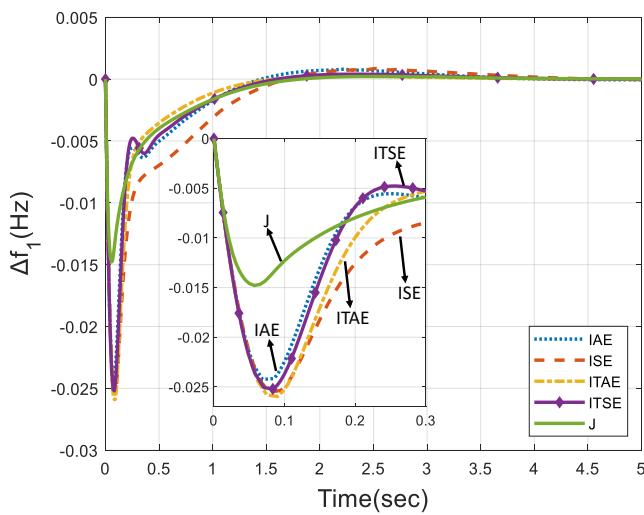
Fig.5 Iteration curve of GSA/IGSA with four main functions

TABLE IV
CONTROLLER PARAMETERS AND FITNESS OF TWO-AREA NON-REHEAT POWER SYSTEM

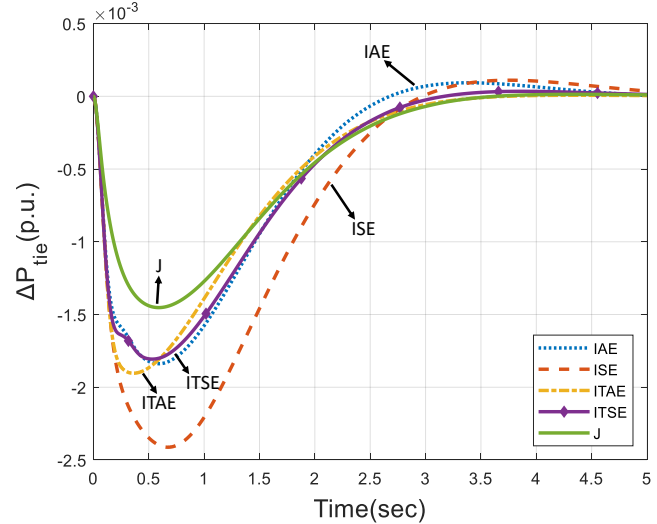
	function	value	K_1	K_2	K_P	K_I	K_D	N
IGSA PID	ITAE	0.1372	-	-	0.8615	1.9999	0.4123	157.0481
	ITSE	0.0070	-	-	1.7466	1.9960	0.8320	162.0389
	ISE	0.0083	-	-	1.9274	1.9995	1.0456	107.9137
	IAE	0.1459	-	-	1.8580	1.9848	0.9825	145.8977
	ITAE	0.0104	0.8775	0.1517	1.7061	1.8588	0.1710	36.5845
GSA FPID	ITSE	3.88×10^{-4}	1.4127	0.0318	1.6123	0.7063	0.3027	128.5547
	ISE	5.66×10^{-4}	0.8804	0.0484	1.4211	1.5126	0.9739	153.2360
	IAE	0.0549	1.9173	0.3494	1.8029	1.4657	0.0346	178.2401
	ITAE	0.0051	1.9420	0.0660	1.7817	1.8675	0.6192	91.1564
	ITSE	5.77×10^{-5}	1.9997	0.0391	1.5767	1.7393	0.6809	165.0154
IGSA FPID	ISE	2.35×10^{-4}	1.9954	0.0687	1.1410	1.3759	0.6291	106.4215
	IAE	0.0140	1.8973	0.0419	1.4764	1.9482	0.7420	138.8145
	J	0.0434	1.9873	0.1448	1.9727	1.9820	0.7950	150.6588

Documents in recent years have proposed many different methods for optimization. In order to prove the superiority of proposed method, the optimal result is compared with others which proposed in documents. Fig.8 are the frequency deviation and tie-line power deviation under different methods, and relational performance index is shown in TABLE V. Those results prove that under the control of IGSA FPID(J), the dynamic performance of controlled system has been improved. The parameters of IGSA FPID(J) are brought into controlled system for simulation, and corresponding function value is calculated again by four main

objective functions. Compared with the values in other documents, all minimums are set by IGSA FPID(J). Performance index is an important reference in evaluating dynamic performance. In all methods used for comparison, the simulation results of proposed method are best in T_s and US . Take Δf_1 as an example, T_s is 1.43 s and US is -0.0151. IACO FPID has best dynamic performance excepts proposed method, and its US is -0.231. Besides, under the control of proposed method, the largest OS and Ess of system response are 2.13×10^{-4} and 3.7×10^{-8} respectively, which are smaller than the standard.

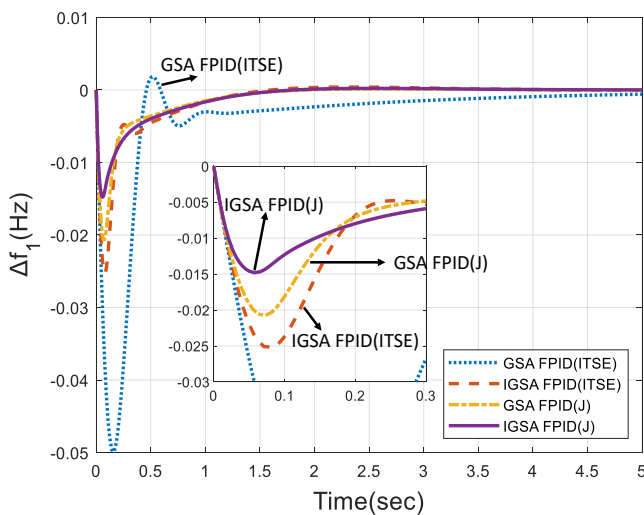


(a) Δf_1

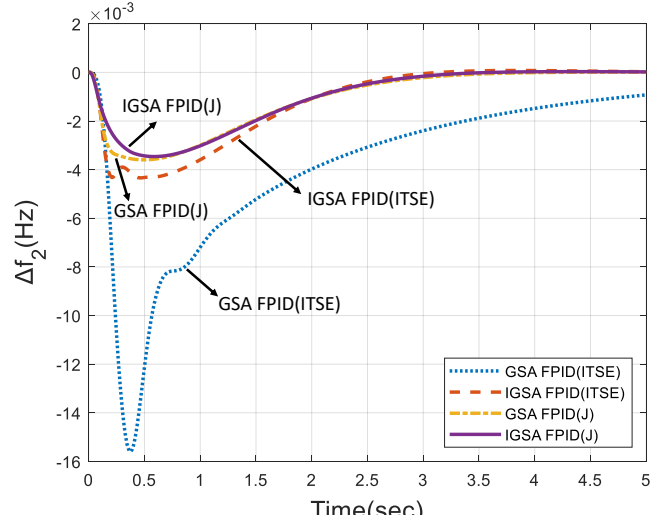


(b) ΔP_{tie}

Fig.6 Frequency deviation and tie-line power deviation for 10% change in area-1 under different objective functions



(a) Δf_1



(b) Δf_2

Fig.7 Frequency deviation for 10% change in area-1 under different improvements

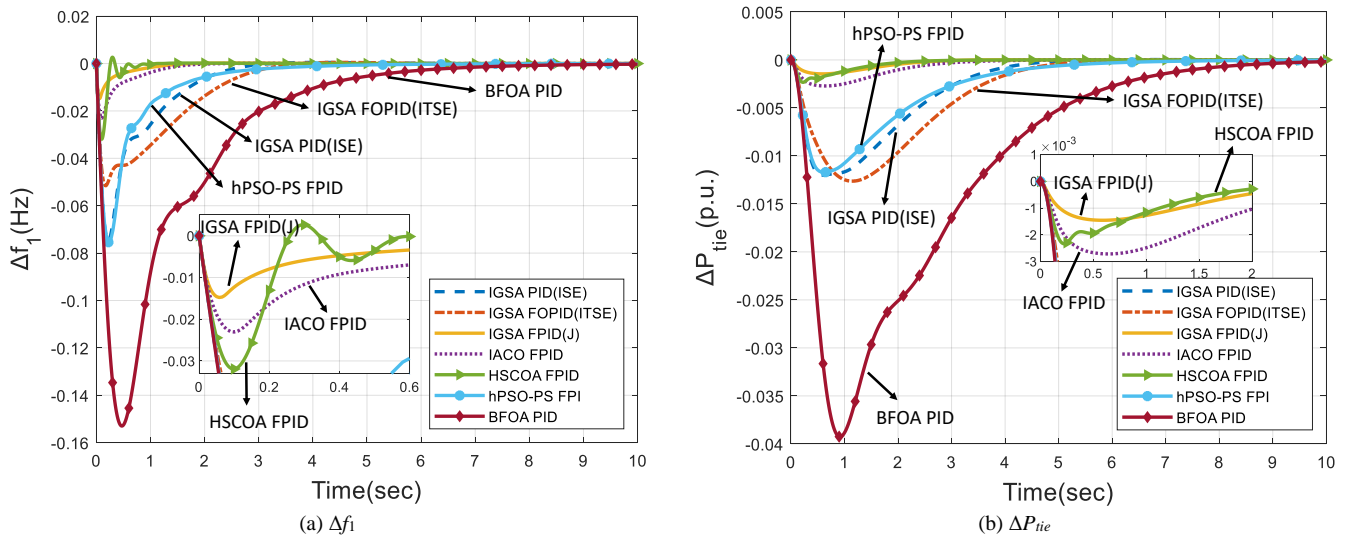


Fig.8 Frequency and tie-line power deviation for 10% change in area-1 under different methods

In addition to excellent dynamic performance, robustness is another standard, which determines stability of controlled system. Controller not only has a good effect on normal systems, but also has enough tolerance and robustness when controlled system changes. Therefore, when the parameters of controller do not change, load and parameters of controlled system are changed (load, T_g , T_i , and T_{12} vary $\pm 50\%$) to simulate the changes or failures in system. Fig.9, Fig.10 and Fig.11 are part of system responses, and TABLE VI lists performance indicators under the different conditions.

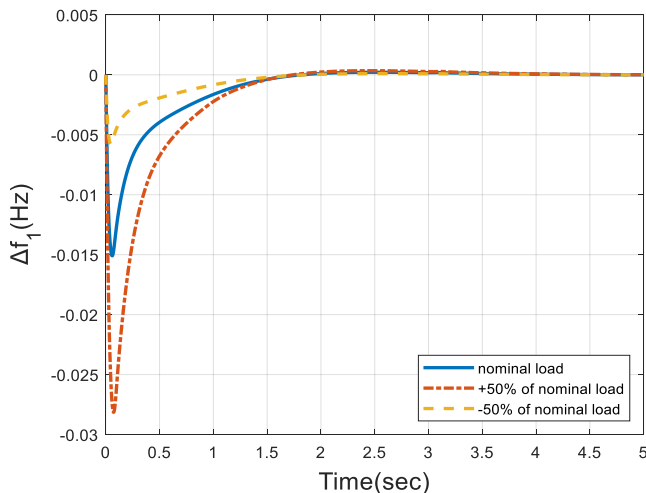


Fig.9 Frequency deviation of Δf_1 for different load change in area-1

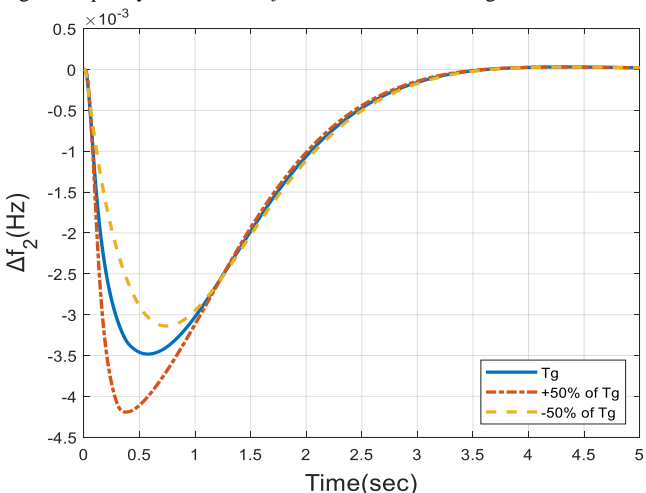


Fig.10 Frequency deviation of Δf_2 in area-1 under different T_g

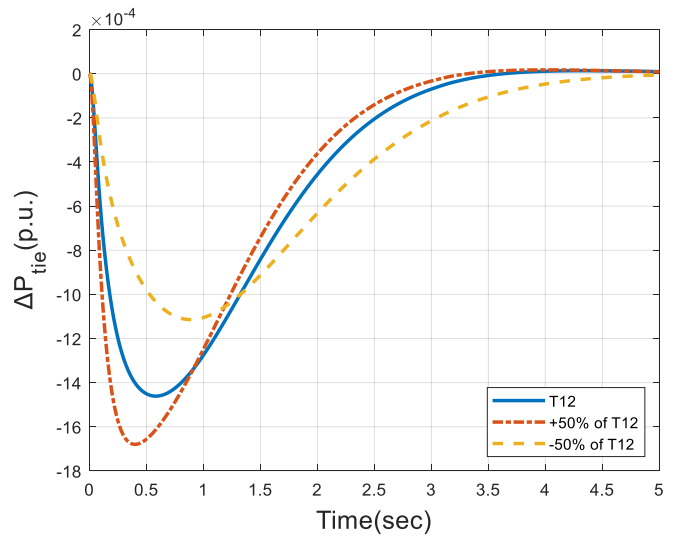


Fig.11 Tie-line power deviation for 10% load in area-1 under different T_{12}

To better explain the stability of system controlled by proposed method, Δf_1 under different load, Δf_2 under different T_g and ΔP_{tie} under different T_{12} are selected to display.

(i) Load change

All indicators show strong positive correlation with load change. The T_s of area-1 is less than 1.5 s, and remaining T_s is generally less than 3 s. Maximum US is 17.83% of nominal load. Those indicators prove the system controlled by proposed method has good ability to resist load change.

(ii) T_g or T_i change

Because some parameters of system have changed, the parameters of controller are not optimal parameters. The change of T_g or T_i has an obvious impact on US and OS , but their response curves gradually overlap. Maximum US is 20.5% of nominal load. It is worth noting that T_g has almost no effect on T_s and Ess , but except for Ess of Δf_2 , T_i has a negative correlation with T_s and Ess to some degree.

(iii) T_{12} change

Compared to previous changes, the change of T_{12} affects all indicators. US is positively correlated with T_{12} , and most of other indicators are negatively correlated with T_{12} . US is less affected by T_{12} , especially US of Δf_1 , which almost has no change. Ess is less than 10^{-7} , which meets the goal of control.

TABLE V
PERFORMANCE INDEX FOR 10% CHANGE IN AREA-1 UNDER DIFFERENT ALGORITHMS

Performance index		Algorithms						
		IGSA PID	IGSA FOPID	IGSA FPID(J)	IACO FPID[13]	HSCOA FPID[23]	hPSO-PS FPI[24]	BFOA PID[4]
Objective function	ITAE	0.1751	0.2669	0.0081	0.0255	0.0883	0.1483	1.1613
	ITSE(10 ⁻³)	6.9756	11.5765	0.0038	0.0093	0.5248	2.5231	115.4239
	IAE(10 ⁻³)	8.3284	10.0296	0.0106	0.0191	2.1885	3.6140	86.9284
Ts (±0.0005)	ISE	0.1448	0.1766	0.0119	0.0273	0.1457	0.0036	0.5840
	Δf ₁	2.98	3.34	1.42	1.78	2.37	5.37	8.85
	Δf ₂	4.70	5.01	2.46	3.20	2.95	6.54	8.52
US	ΔP _{tie}	4.28	4.73	1.93	2.59	1.22	5.28	9.94
	Δf ₁	-0.0748	-0.0516	-0.0151	-0.0231	-0.0319	-0.0776	-0.1530
	Δf ₂	-0.0333	-0.0312	-0.0035	-0.0066	-0.0061	-0.0305	-0.0393
OS	ΔP _{tie}	-0.0120	-0.0126	-0.0014	-0.0027	-0.0026	-0.0124	-0.1089
	Δf ₁	4.72×10 ⁻⁴	4.84×10 ⁻⁴	2.13×10 ⁻⁴	6.78×10 ⁻⁵	3.54×10 ⁻³	0	0
	Δf ₂	4.36×10 ⁻⁵	4.77×10 ⁻⁶	3.08×10 ⁻⁵	0	4.87×10 ⁻⁴	0	0
Ess	ΔP _{tie}	3.93×10 ⁻⁵	2.03×10 ⁻⁶	1.36×10 ⁻⁵	3.44×10 ⁻⁹	1.02×10 ⁻⁵	0	0
	Δf ₁	-2.35×10 ⁻⁶	4.91×10 ⁻⁶	3.71×10 ⁻⁸	-5.70×10⁻¹⁶	2.16×10 ⁻⁶	-2.58×10 ⁻⁵	-2.53×10 ⁻⁴
	Δf ₂	2.72×10 ⁻⁶	4.77×10 ⁻⁶	-1.86×10 ⁻⁸	-1.91×10⁻¹⁵	1.86×10 ⁻⁵	-5.15×10 ⁻⁵	-1.77×10 ⁻⁴
	ΔP _{tie}	1.74×10 ⁻⁶	2.03×10 ⁻⁶	-1.01×10 ⁻⁸	-5.23×10⁻¹⁶	-7.47×10 ⁻⁷	-2.14×10 ⁻⁵	-4.83×10 ⁻⁴

TABLE VI
PERFORMANCE INDEX FOR 10% CHANGE IN AREA-1 UNDER DIFFERENT CONDITION

Variable parameter	Change	Ts (±0.0005)			US			OS			Ess		
		Δf ₁	Δf ₂	ΔP _{tie}	Δf ₁	Δf ₂	ΔP _{tie}	Δf ₁	Δf ₂	ΔP _{tie}	Δf ₁	Δf ₂	ΔP _{tie}
Nominal	None	1.42	2.46	1.93	-0.0151	-0.0035	-0.0014	2.13×10 ⁻⁴	3.08×10 ⁻⁵	1.36×10 ⁻⁵	3.71×10 ⁻⁸	1.86×10 ⁻⁸	-1.01×10 ⁻⁸
	+50%	1.46	2.71	2.25	-0.0281	-0.0067	-0.0028	3.45×10 ⁻⁴	4.44×10 ⁻⁵	2.00×10 ⁻⁵	5.80×10 ⁻⁸	-2.99×10 ⁻⁸	-1.62×10 ⁻⁸
Load	-50%	1.22	2.00	1.21	-0.0058	-0.0015	-0.0006	1.02×10 ⁻⁴	1.57×10 ⁻⁵	6.93×10 ⁻⁶	1.81×10 ⁻⁸	-8.84×10 ⁻⁹	4.83×10 ⁻⁹
	+50%	1.35	2.43	1.91	-0.0205	-0.0042	-0.0017	2.21×10 ⁻⁴	3.07×10 ⁻⁵	1.41×10 ⁻⁵	3.65×10 ⁻⁸	-1.77×10 ⁻⁸	-9.47×10 ⁻⁹
T _g	-50%	1.49	2.50	1.96	-0.0091	-0.0031	-0.0013	2.09×10 ⁻⁴	3.10×10 ⁻⁵	1.33×10 ⁻⁵	3.73×10 ⁻⁸	-1.94×10 ⁻⁸	-1.06×10 ⁻⁸
	+50%	1.11	2.29	1.83	-0.0221	-0.0052	-0.0021	3.15×10 ⁻⁴	3.97×10 ⁻⁵	1.97×10 ⁻⁵	3.86×10 ⁻⁸	-1.20×10 ⁻⁸	-6.49×10 ⁻⁹
T _t	-50%	1.66	2.65	2.07	-0.0083	-0.0028	-0.0012	1.77×10 ⁻⁴	2.79×10 ⁻⁵	1.09×10 ⁻⁵	2.80×10 ⁻⁸	-2.62×10 ⁻⁸	-1.21×10 ⁻⁸
	+50%	1.58	2.29	1.79	-0.0150	-0.0040	-0.0017	1.14×10 ⁻⁴	4.00×10 ⁻⁵	1.75×10 ⁻⁵	2.17×10 ⁻⁸	-4.37×10 ⁻⁹	-3.25×10 ⁻⁹
T ₁₂	-50%	3.11	2.99	2.25	-0.0152	-0.0026	-0.0011	6.51×10 ⁻⁴	0	1.77×10 ⁻⁷	7.24×10 ⁻⁸	-5.44×10 ⁻⁸	-2.57×10 ⁻⁸
	+50%	3.11	2.99	2.25	-0.0152	-0.0026	-0.0011	6.51×10 ⁻⁴	0	1.77×10 ⁻⁷	7.24×10 ⁻⁸	-5.44×10 ⁻⁸	-2.57×10 ⁻⁸

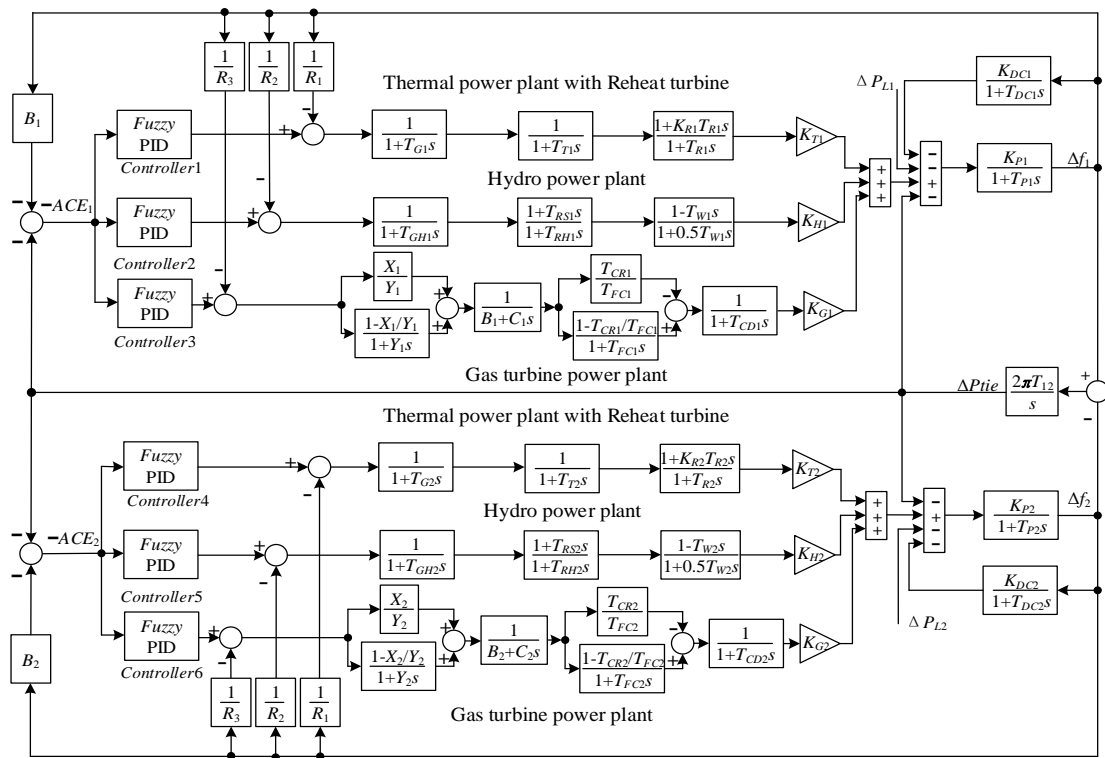


Fig.12 Two-area multi-source power system

TABLE VII
CONTROLLER PARAMETERS OF TWO-AREA MULTI-SOURCE POWER SYSTEM

System model		K ₁	K ₂	K _P	K _I	K _D	N
With HVDC	Thermal	-1.9933	-0.1678	-1.9992	-1.4081	-0.6537	88.0642
	Hydro	-0.9805	-0.3256	1.0193	1.2098	0.1426	48.3380
	Gas	0.8093	1.3668	1.6927	0.5165	0.3668	82.3676
Without HVDC	Thermal	1.9010	0.1028	1.8503	1.8410	0.4599	95.7775
	Hydro	0.6785	-0.1517	0.7632	1.0669	0.2548	179.4175
	Gas	1.4407	-0.9263	-0.2952	-0.2323	0.0517	161.9774

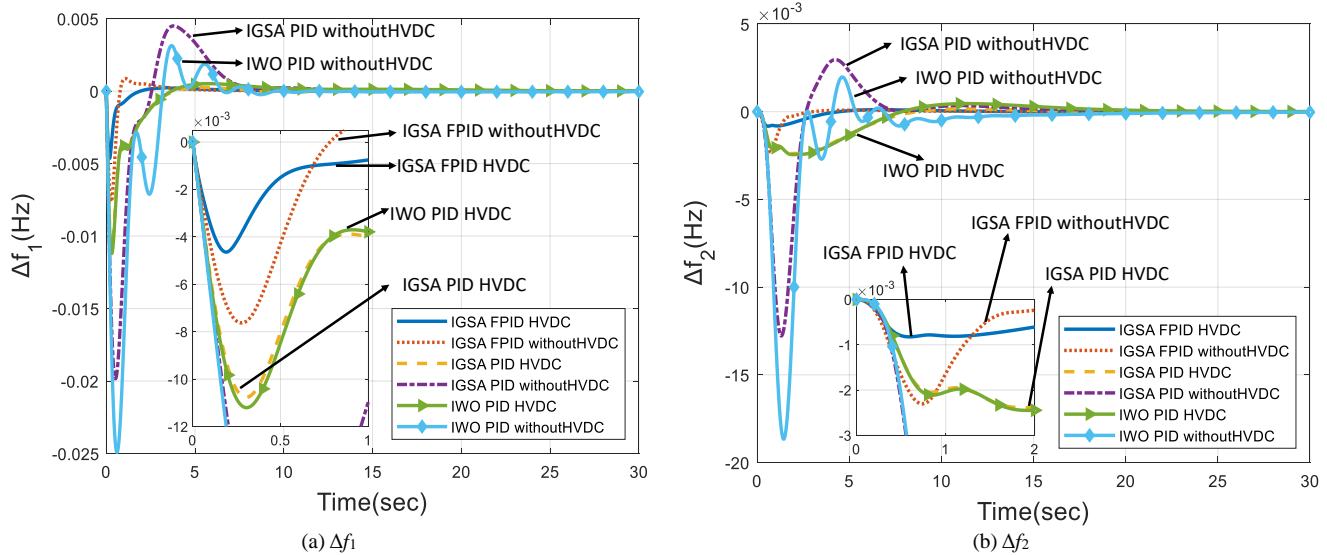


Fig.13 Frequency deviation for 1% load in area-1 under different methods

TABLE VIII
PERFORMANCE INDEX OF TWO-AREA MULTI-SOURCE SYSTEM UNDER DIFFERENT CASES

Change	Performance index	HVDC			Without HVDC				
		IGSA FPID	IGSA PID	IWO PID [15]	IGSA FPID	IGSA PID	IWO PID		
Case1 load1=0.01 p.u. load2=0 p.u.	$T_s(s)$ (± 0.0005)	Δf_1	1.22	3.07	6.27	2.12	7.26	6.26	
		Δf_2	2.32	6.72	6.56	1.45	6.54	9.98	
		ΔP_{tie}	0	4.78	8.97	1.01	3.8	9.36	
	US	Δf_1	-0.0046	-0.0108	-0.0112	-0.0076	-0.0199	-0.0249	
		Δf_2	-0.0008	-0.0024	-0.0024	-0.0023	-0.0128	-0.0187	
		ΔP_{tie}	-0.0004	-0.0017	-0.0018	-0.0007	-0.0030	-0.0040	
	OS	Δf_1	2.37×10^{-4}	2.64×10^{-4}	5.17×10^{-4}	8.71×10^{-4}	4.50×10^{-3}	3.14×10^{-3}	
		Δf_2	1.13×10^{-4}	1.65×10^{-4}	4.61×10^{-4}	8.69×10^{-5}	2.97×10^{-3}	1.97×10^{-3}	
		ΔP_{tie}	5.61×10^{-5}	2.75×10^{-4}	5.00×10^{-4}	4.16×10^{-5}	4.43×10^{-4}	1.07×10^{-4}	
	Ess	Δf_1	2.52×10^{-6}	-1.54×10^{-5}	6.84×10^{-6}	1.65×10^{-5}	-2.08×10^{-6}	-3.51×10^{-5}	
		Δf_2	5.38×10^{-6}	-9.58×10^{-6}	8.25×10^{-6}	3.45×10^{-5}	5.77×10^{-5}	-2.59×10^{-5}	
		ΔP_{tie}	1.99×10^{-6}	-5.63×10^{-6}	4.52×10^{-6}	1.81×10^{-5}	-5.41×10^{-6}	1.02×10^{-4}	
	Case2 load1=0.02 p.u. load2=0 p.u.	$T_s(s)$ (± 0.0005)	Δf_1	1.57	5.82	8.98	3.45	8.01	7.79
			Δf_2	3.34	7.49	15.86	2.1	13.27	12.46
			ΔP_{tie}	2.27	9.82	12.58	1.79	13.68	11.81
US		Δf_1	-0.0095	-0.0215	-0.0224	-0.0170	-0.0397	-0.0499	
		Δf_2	-0.0018	-0.0048	-0.0049	-0.0057	-0.0256	-0.0373	
		ΔP_{tie}	-0.0009	-0.0035	-0.0036	-0.0018	-0.0061	-0.0080	
OS		Δf_1	4.38×10^{-4}	5.27×10^{-4}	1.03×10^{-3}	2.93×10^{-3}	9.00×10^{-3}	6.28×10^{-3}	
		Δf_2	2.05×10^{-4}	3.29×10^{-4}	9.23×10^{-4}	1.50×10^{-4}	5.94×10^{-3}	3.95×10^{-3}	
		ΔP_{tie}	1.03×10^{-4}	5.49×10^{-4}	1.00×10^{-3}	7.55×10^{-5}	8.86×10^{-4}	2.13×10^{-4}	
Ess		Δf_1	4.45×10^{-6}	-3.08×10^{-5}	1.37×10^{-5}	2.50×10^{-5}	-4.16×10^{-6}	-7.02×10^{-5}	
		Δf_2	1.01×10^{-5}	-1.92×10^{-5}	1.65×10^{-5}	5.99×10^{-5}	1.15×10^{-4}	-5.17×10^{-5}	
		ΔP_{tie}	3.73×10^{-6}	-1.13×10^{-5}	9.05×10^{-6}	3.39×10^{-5}	-1.08×10^{-5}	2.04×10^{-4}	
Case3 load1=0.01 p.u. load2=0.01 p.u.		$T_s(s)$ (± 0.0005)	Δf_1	2.1	6.15	13.73	1.08	11.52	9.89
			Δf_2	2.1	6.15	13.73	1.08	11.52	9.89
			ΔP_{tie}	0	0	0	0	0	0
	US	Δf_1	-0.0048	-0.0112	-0.0116	-0.0082	-0.0234	-0.0305	
		Δf_2	-0.0048	-0.0112	-0.0116	-0.0082	-0.0234	-0.0305	
		ΔP_{tie}	0	0	0	0	0	0	
	OS	Δf_1	2.25×10^{-4}	1.31×10^{-4}	6.04×10^{-4}	3.21×10^{-4}	7.31×10^{-3}	2.21×10^{-3}	
		Δf_2	2.25×10^{-4}	1.31×10^{-4}	6.04×10^{-4}	3.21×10^{-4}	7.31×10^{-3}	2.21×10^{-3}	
		ΔP_{tie}	8.96×10^{-20}	1.98×10^{-19}	4.71×10^{-19}	0	0	0	
	Ess	Δf_1	7.94×10^{-6}	-2.50×10^{-5}	1.51×10^{-5}	5.46×10^{-5}	5.56×10^{-5}	-6.10×10^{-5}	
		Δf_2	7.94×10^{-6}	-2.50×10^{-5}	1.51×10^{-5}	5.46×10^{-5}	5.56×10^{-5}	-6.10×10^{-5}	
		ΔP_{tie}	-6.52×10^{-20}	-1.76×10^{-19}	-4.05×10^{-20}	0	0	0	

Under the condition of 1% load disturbance at $t=0$ s in area-1, the optimal parameters are listed in TABLE VII, and relevant responses and performance index are shown in Fig.13, Fig.14, and TABLE VIII.

(i) Comparison and analysis of different methods

The superiority of proposed method is reflect by system responses, because the response named IGSA FPID has all best indicators. Under the control of IGSA FPID, the system with HVDC has smaller US and OS , and System without

HVDC is better in Ess . Comparing the indicators of IGSA FPID with those of IGSA PID and IWO PID, the former is superior in all US and most T_s . Comparing the performance index under the control of FPID and PID, most indicators of the former are 30% of the latter, and maximum US of the former is 46% of nominal load.

(ii) Comparison and analysis of different load

Load change is a common method to verify general applicability of proposed method. The load change of case2 is

two times that of case1. *OS* and *Ess* are more than two times, but *US* and *Ts* are less than two times. However, *US* and *Ts* have a greater impact on the controlled system than *OS* and *Ess* because of their larger values. The ratio of change in *US* and *Ts* is smaller than the one of load change, and it will decrease when load change increases. Which means when a large percentage of load change comes out, the tolerance of complex system is better than simple system.

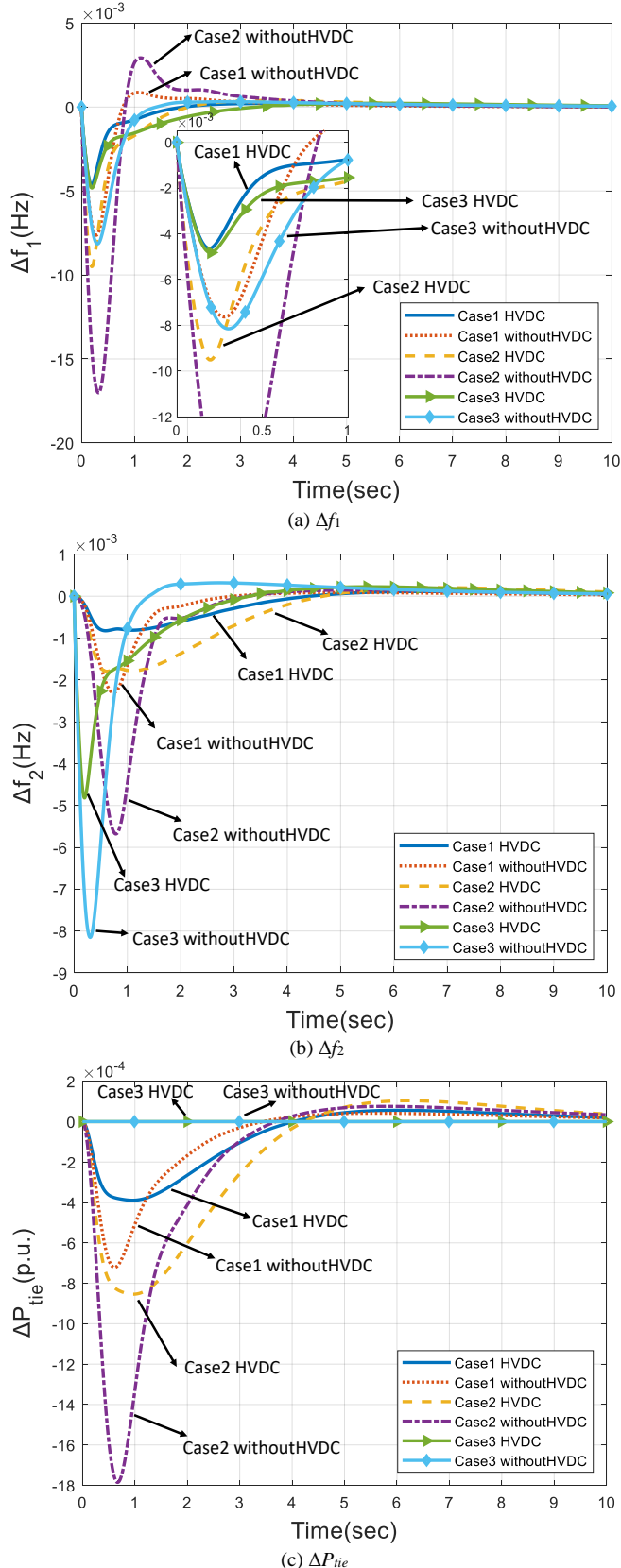


Fig.14 Frequency and tie-line power deviation under different cases

(iii) Analysis of the influence of HVDC

HVDC has an effect on reducing *US*. Traditional system with AC links has good dynamic performance and can quickly return to normal state after being disturbed. The response of system with HVDC and traditional AC link are shown in Fig.14. When system is equipped with HVDC, the *US* of frequency and tie-line power decrease. Under the same load change, the former is about 50% of the latter, which also proves that HVDC can effectively suppress fluctuations and enhance stability of power systems.

In order to test the robustness of controlled system and the influence of HVDC in a more realistic environment, a random load in Fig.15 is used in area-1. The random load is composed of two parts, one is continuous and small load change, and the other is intermittent and large change. Fig.16 is the response of Δf_1 , which shows the performance of controller and the response of controlled system are degraded. According to results, some conclusions are drawn.

(i) In the system without HVDC, when load change increases, the ratio of *US* and *OS* to nominal load will increase. For example, at time = 10 s, the percentage of maximum *US* (0.042) to nominal load (0.08) is 51% and at time = 60 s, the ratio of maximum *US* (0.116) to nominal load (0.17) is 68.2%. While in the system with HVDC, the ratios of maximum *US* to nominal load are 32.5% and 32.4% respectively.

(ii) Under random load change, the effect of HVDC in suppressing fluctuations is more obvious. At time = 60 s, ΔP_L in area-1 changes from -0.05 to 0.12, while the Δf_1 of the system with HVDC has smaller *US*. Its *OS* is 0.005, but the *OS* of Δf_1 of the system without HVDC is 0.065.

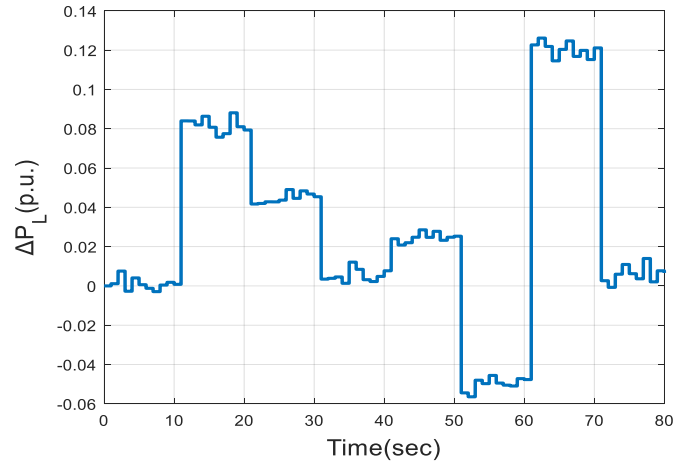
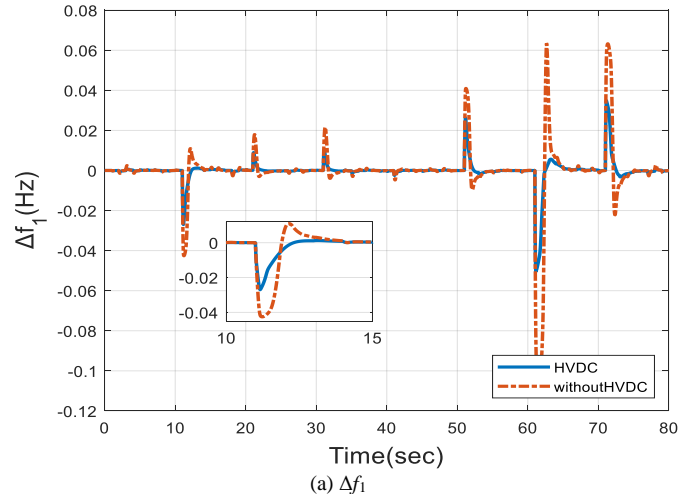


Fig.15 Random load change in area-1



(a) Δf_1

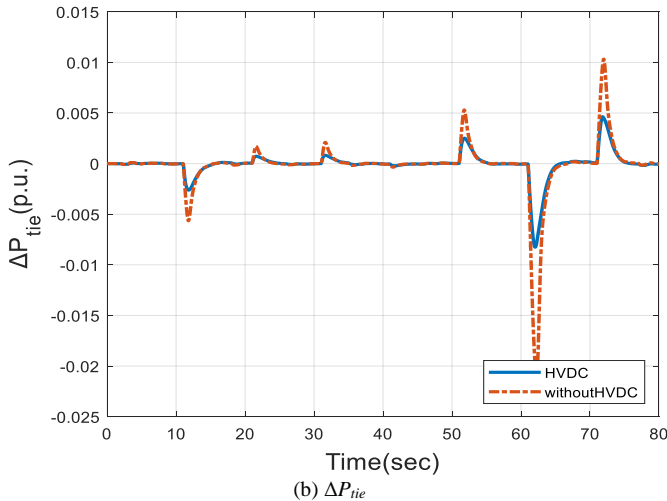


Fig.16 Frequency deviation and Tie-line power deviation for random change in area-1 under IGSA FPID

C. Three-area unequal power system with GDB and GRC connected wind turbines

Wind power is random and uncertain, and it cannot be an independent unit of power supply. Controllable energies such as thermal power are usually used as backup energies to enhance the stability of wind power. LFC is a main challenge that wind power is connected into power systems. In order to simulate the multi-area system with WT, a three-area power system with GDB and GRC connected WT is designed and controlled by proposed method.

(i) Wind turbine (WT)

WT has many equivalent models. From the flow of control, its model can be equivalent to three parts: pitch angle control, hydraulic servo actuator and mechanical structure. Its equivalent model is shown in Fig.17, and corresponding derivation is elaborated in [25].

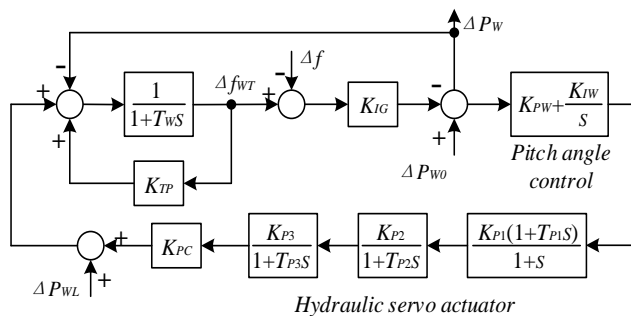


Fig.17 Equivalent wind turbine model

(ii) Governor dead band (GDB)

The governor adjusts the output (torque) of prime mover so that frequency and power can keep stable. But governor has a dead zone, which means when input is lower than nominal limit, valve will no longer act. GDB consists of two parts: Inherent GDB is caused by the error of mechanical structure, and intentional GDB is set artificially to avoid mechanical loss caused by frequent actions. The maximum of GDB is 0.06% [3].

(iii) Generation rate constraint (GRC)

In real power system, due to the limitations of mechanical structure and keeping generators from being damaged because of violent changes, the change of output (torque) must be limited within a given range. This limitation is named

GRC. In general, the typical constraint of thermal power is 3%/min [3], and for hydropower plants, it is 270%/min.

The model is shown in Fig.18 and relevant parameters are listed in Appendix C. ω_3 is adjusted to 50 to make IGSA: FPID has better ability to inhibit OS. The range of K_{PW} and K_{TW} are [0, 2], and other conditions are equal.

In this study, for three-area system which takes thermal power as backup energy, the influence of GDB, GRC and WT are analyzed individually. Under the condition of 1% load change at $t=0$ s in area-1, the parameters of controller are optimized by proposed method, and parameters are listed in TABLE IX. Those parameters are used in simulations under different conditions. All performance indicators are shown in TABLE X and some response curves are shown in Fig.19. Some conclusions are made through these simulation results.

(i) Compared with two-area non-reheat power system, the performance of controller in three-area reheat system decreases, but it still has good dynamic performance. The maximum US is 38.6% of nominal load, and all OS and Ess are less than or equal to 10^{-6} . It is proved that under same proportional load change, the impact of load change increases with the complexity of system. However, a complex system always has a large capacity, and the ratio of same load change to system capacity is smaller, so a complex system with high capacity is usually more stable.

(ii) Comparing the data of case1 and case2, nonlinear factors such as GDB and GRC have a significant impact on dynamic performance. Under the same condition, all T_s of the nonlinear system with GDB and GRC are smaller than that of the linear system, especially in Δf_1 , Δf_2 , and ΔP_{12} . T_s of ΔP_{12} has the largest difference and its ratio is 3.3. Besides, US of the former are 4 times larger than the latter, and except for OS of Δf_1 , all OS of the former are 10 times larger than the latter.

(iii) Comparing the data of case1 and case3, WT has positive influence on system. In the linear system with WT, all indicators are better than the linear system, which is more obvious in T_s and US . In terms of OS , the largest OS is 1.12×10^{-4} , which is 2.12% of nominal disturbance and it is smaller than standard of Ess .

(iv) The comparison between Case2 and Case4 shows that under the constraint of nonlinearity, the system with WT is more capable of restraining US . US of system with WT is 25% of the one of system without WT. All T_s have been significantly reduced, which is better reflected in tie-line power deviation (Δf_3 , ΔP_{12} , and ΔP_{13}). Meanwhile, some OS and all Ess decrease significantly, although some OS is increase, they can also quickly fall back to nominal value.

In general, in a system without nonlinear constraints, WT significantly improves performance of controlled system. While in a system with constraints, some indicators (T_s , US , Ess) are significantly reduced. Some OS increase, but most of them are within nominal standard of Ess . Therefore, these analyses reveal that the connection of WT effectively reduces performance index and has a positive effect on system stability and dynamic performance.

Usually, the real load is high-frequency and random. To further evaluate the stability of controlled system, high-frequency load change is introduced in three-area power system with GDB, GRC and WT, and some system responses

are shown in Fig.20. The amplitude of most random loads is in [-0.2, 0.2]. Area-1 is directly affected by the random load, but the fluctuation of area-1 is less than 0.03. The fluctuations of other areas affected indirectly by area-1 are so small that they

can be ignored. Those results show that under the control of IGSA FPID, the three-area system still has good resistance to high-frequency disturbances, and the resistance gradually increases with the expansion of the system.

TABLE IX
CONTROLLER PARAMETERS OF THREE-AREA POWER SYSTEM UNDER DIFFERENT CONDITIONS

Difference	area	K_1	K_2	K_P	K_I	K_D	N
With none	1	1.5643	0.2608	1.0815	0.1561	0.2587	94.8794
	2	0.4982	0.0310	0.2325	0.6636	1.6742	154.1586
	3	1.5519	0.3326	0.3901	1.4848	0.2354	111.0099
With GDB GRC	1	0.4340	0.6062	0.7576	0.8362	0.3962	11.4195
	2	1.6268	0.4249	0.9334	0.6348	0.1363	127.4961
	3	0.7741	0.3481	0.9979	0.3665	0.5339	130.4588
With WT	1	1.8092	0.1062	1.1709	1.1679	0.5023	117.9253
	2	1.8467	0.1707	1.7019	1.7587	0.0563	55.8235
	3	1.4963	1.6801	0.1673	0.0839	0.0545	36.9108
	WT	-	-	1.0786	1.5686	-	-
With WT GDB GRC	1	1.8871	1.4140	1.0515	1.0853	0.3883	119.4965
	2	1.2901	0.0894	0.9345	1.7702	1.7855	119.6977
	3	0.9579	0.0653	0.8765	0.6916	0.6884	3.0053
	WT	-	-	0.1718	0.0759	-	-

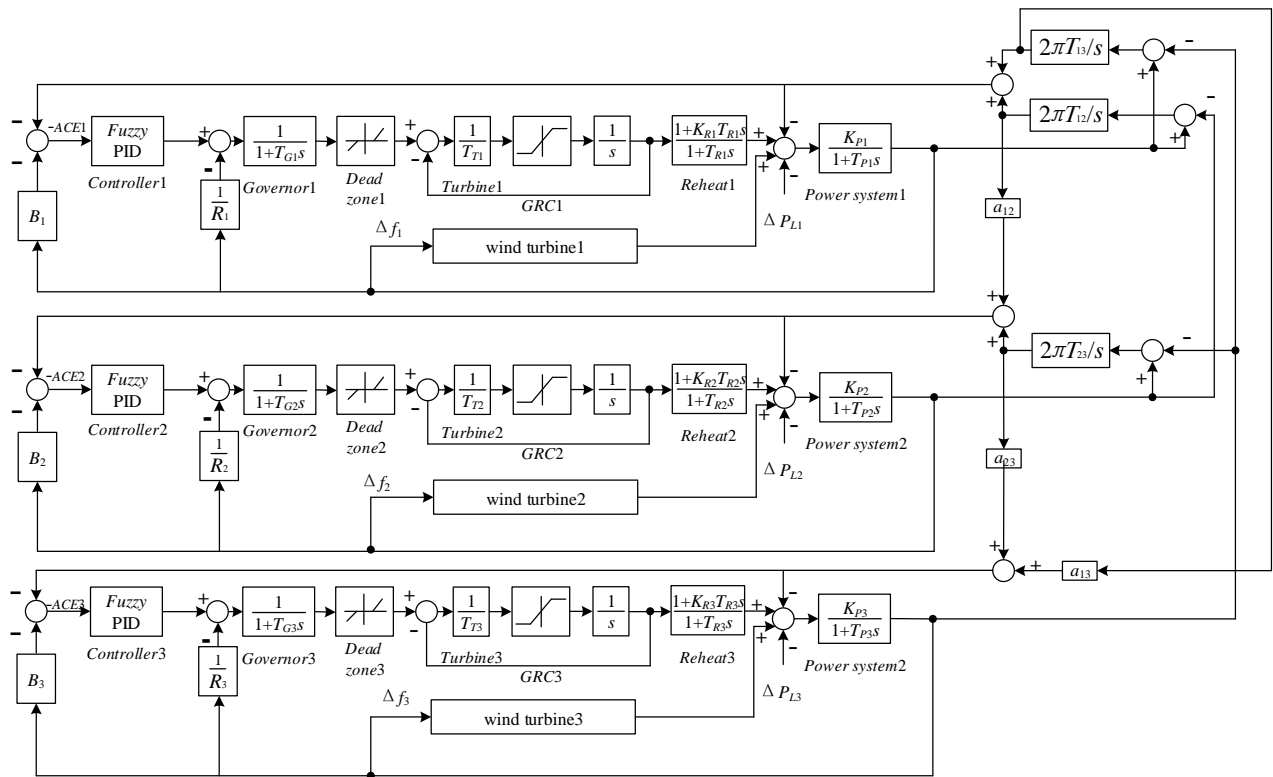
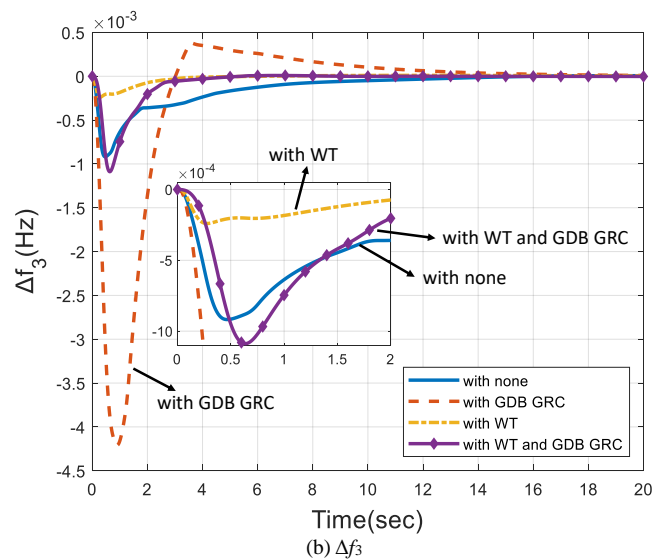
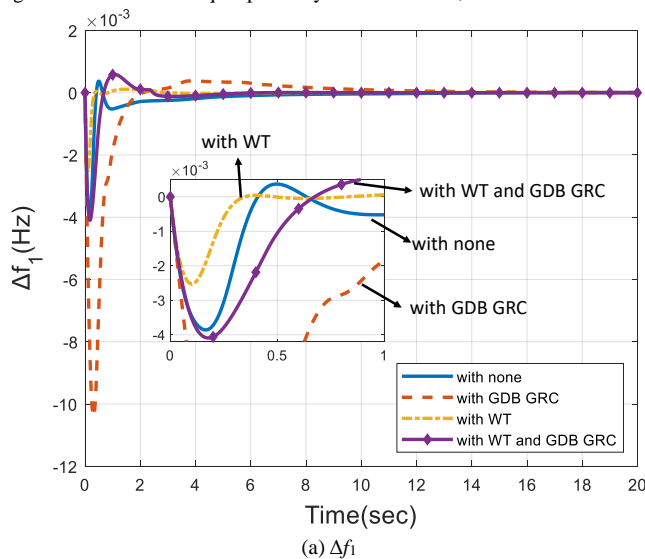


Fig.18 Three-area unequal power system with GDB, GRC connected WT



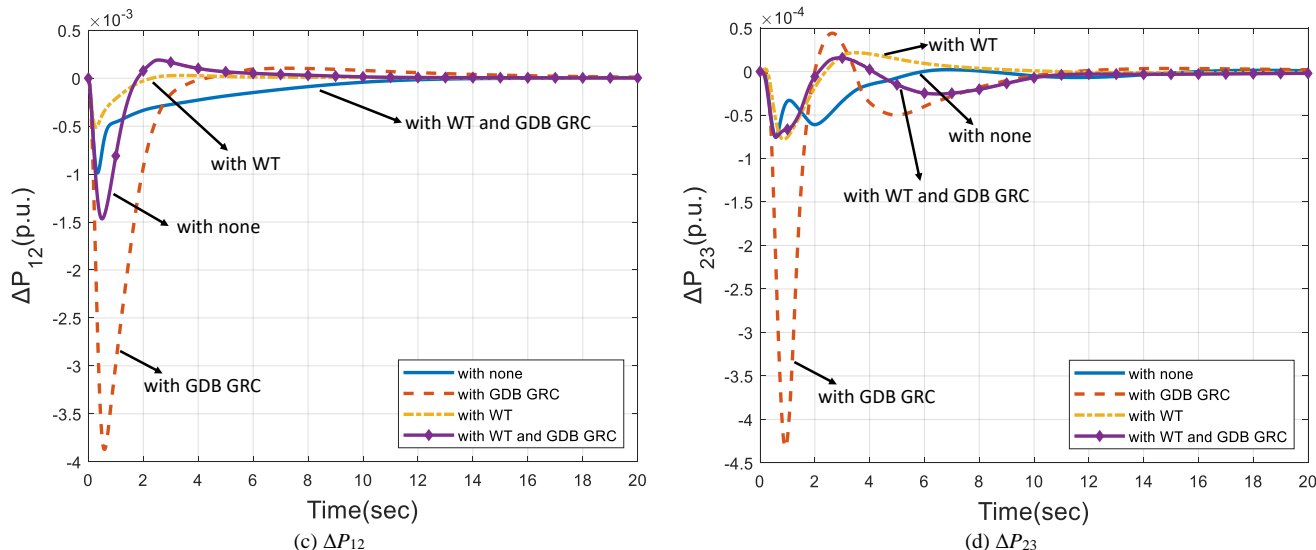
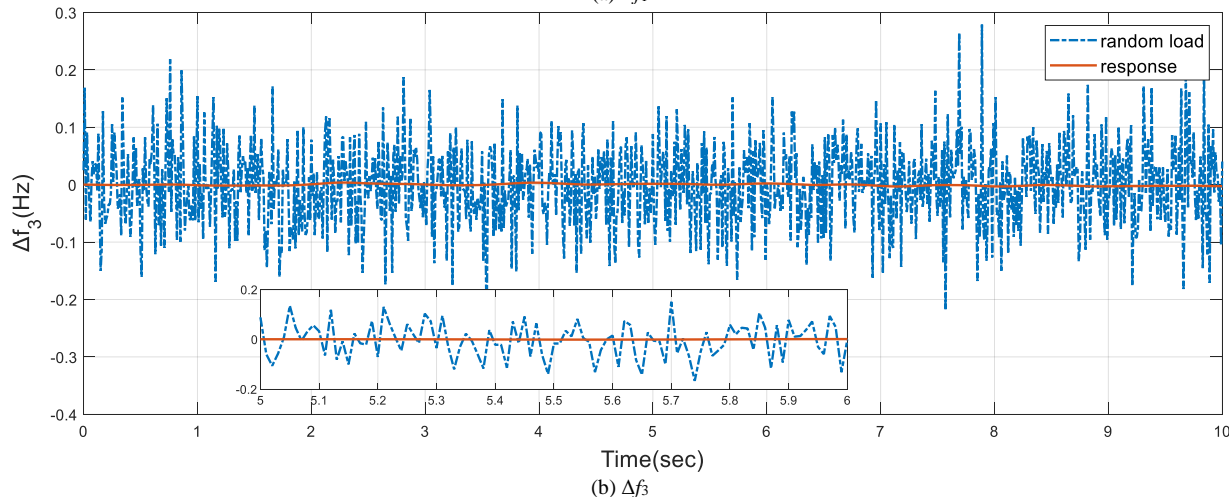
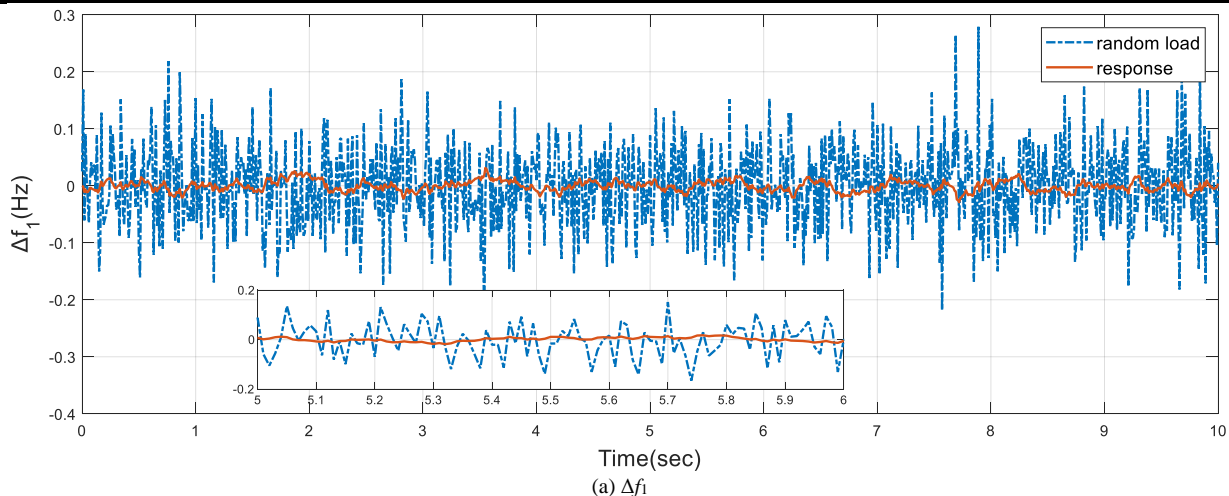


Fig.19 Frequency deviation and Tie-line power deviation for 1% change in area-1 under different conditions

TABLE X
PERFORMANCE INDEX OF THREE-AREA POWER SYSTEM UNDER DIFFERENT CONDITIONS

	Case1: With none						Case2: With GDB GRC					
	Δf_1	Δf_2	Δf_3	ΔP_{12}	ΔP_{13}	ΔP_{23}	Δf_1	Δf_2	Δf_3	ΔP_{12}	ΔP_{13}	ΔP_{23}
T_s	1.1	1.48	1.31	0.73	2.35	0	1.48	2.47	2.5	2.38	2.42	0
US	-3.86×10^{-3}	-1.21×10^{-3}	-9.18×10^{-4}	-9.88×10^{-4}	-1.31×10^{-3}	-7.58×10^{-5}	-1.04×10^{-2}	-5.09×10^{-3}	-4.21×10^{-3}	-3.87×10^{-3}	-5.38×10^{-3}	-4.32×10^{-4}
OS	3.71×10^{-4}	6.32×10^{-6}	6.72×10^{-6}	5.48×10^{-6}	8.61×10^{-6}	2.21×10^{-6}	3.77×10^{-4}	3.13×10^{-4}	3.78×10^{-4}	1.05×10^{-4}	9.43×10^{-5}	4.41×10^{-5}
Ess	7.17×10^{-6}	5.93×10^{-6}	6.55×10^{-6}	5.48×10^{-6}	8.61×10^{-6}	8.41×10^{-7}	6.58×10^{-6}	8.54×10^{-6}	9.00×10^{-6}	1.11×10^{-5}	1.81×10^{-5}	2.05×10^{-6}
	Case3: With WT						Case4: With GDB GRC WT					
	Δf_1	Δf_2	Δf_3	ΔP_{12}	ΔP_{13}	ΔP_{23}	Δf_1	Δf_2	Δf_3	ΔP_{12}	ΔP_{13}	ΔP_{23}
T_s	0.25	0.42	0	0.31	0.77	0	1.296	1.224	1.329	1.205	1.36	0
US	-2.53×10^{-3}	-5.00×10^{-4}	-2.40×10^{-4}	-5.11×10^{-4}	-6.41×10^{-4}	-7.81×10^{-5}	-4.10×10^{-3}	-1.08×10^{-3}	-1.09×10^{-3}	-1.47×10^{-3}	-1.98×10^{-3}	-7.49×10^{-5}
OS	1.12×10^{-4}	1.01×10^{-5}	1.07×10^{-5}	2.89×10^{-5}	8.11×10^{-5}	2.16×10^{-5}	5.89×10^{-4}	1.34×10^{-5}	9.00×10^{-6}	1.90×10^{-4}	2.66×10^{-4}	1.57×10^{-5}
Ess	4.32×10^{-6}	4.55×10^{-6}	4.33×10^{-6}	1.48×10^{-6}	-1.96×10^{-7}	-9.82×10^{-7}	-1.76×10^{-6}	-1.47×10^{-6}	-1.75×10^{-6}	3.14×10^{-6}	-3.19×10^{-7}	-2.04×10^{-6}



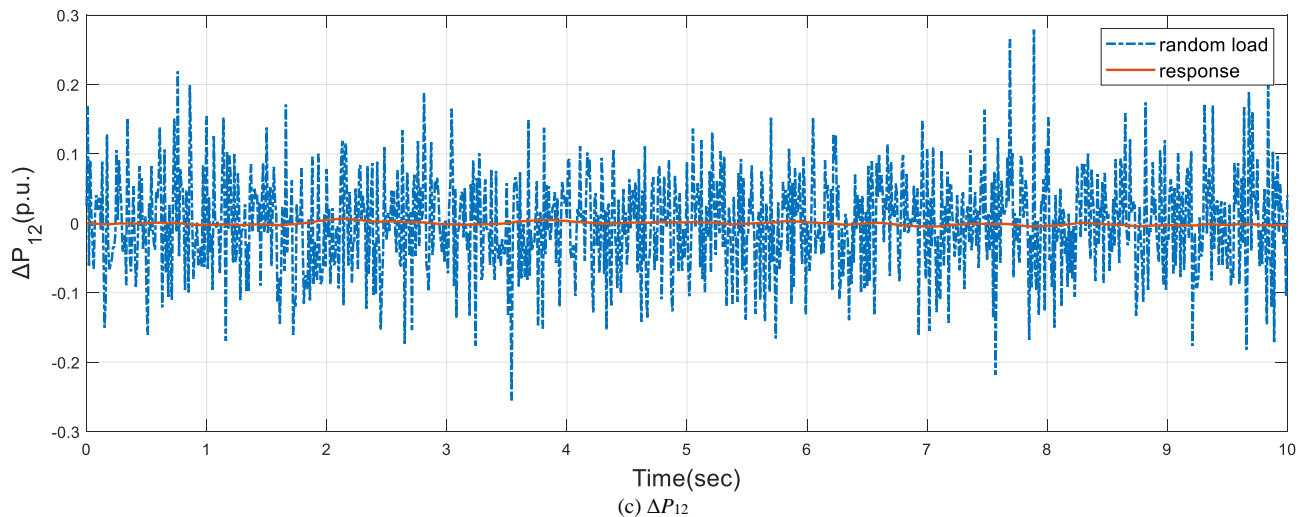


Fig.20 Frequency deviation and tie-line power deviation for high-frequency load in area-1

IV. CONCLUSION

In this paper, IGSA calculated with an objective function considering performance index is used to optimize the parameters of FPID controller. Firstly, six standard functions are used to prove that the selected algorithm is reasonable and the proposed improvement measures are effective. Secondly, a typical two-area non-reheat system is controlled and tested by IGSA FPID, and effectiveness of improved measures for GSA is verified in terms of iteration speed and accuracy of results. Compared with those results of IACO, HSCOA, hPSO-PS, BFOA and other methods proposed in recent years, its T_s and US are about 60%-80% of remaining smallest value, and its maximum US is 0.0151, which is only 15.1% of nominal load. Robustness analysis is realized by varying load and system parameters. When system parameters change $\pm 50\%$ of nominal value, the change of T_s is less than 0.5 s, and the change of overshoot is less than 0.02. These results prove that after controlled system changes, FPID optimized by IGSA still has excellent control and controller parameters doesn't need to be adjusted in real time, thereby the burden on central processing unit is reduced. Thirdly, in the two-area multi-source system with thermal power, hydropower and gas turbines, IGSA: FPID completely surpasses other methods in terms of US and OS , and corresponding performance indicators are 30% of other methods. Besides, the results show that HVDC can reduce US , suppress OS , and shorten T_s . What's more, random load verifies stability of controlled system and further prove the effect of HDVC in suppressing fluctuations. Finally, in the three-area unequal reheat system with GDB and GRC, Its response curves and performance index show that the impact of nonlinear constraints on dynamic performance is obvious, but regardless of whether nonlinear constraints are considered, WT can reduce system fluctuation and increase dynamic performance. Therefore, FPID controller optimized by IGSA has excellent control effects, stability and universal applicability. Moreover, the application of new energy and being connected to power grids is an inevitable trend. Therefore, LFC still needs more in-depth and more practical research.

APPENDIX

A. Two-area non-reheat power system [4, 13, 23]

$f = 60$ Hz; $P_{R1} = P_{R2} = 2000$ MW; $B_1 = B_2 = 0.425$ p.u.MW/Hz; $R_1 = R_2 = 2.4$ Hz/p.u.; $T_{G1} = T_{G2} = 0.08$ s; $T_{T1} = T_{T2} = 0.3$ s; $K_{PS1} = K_{PS2} = 120$ Hz/p.u.MW; $T_{PS1} = T_{PS2} = 20$ s; $T_{12} = 0.545$ p.u.; $a_{12} = -P_{R1} = P_{R2} = -1$.

B. Two-area multi-source power system with HVDC [15]

$f = 60$ Hz; $P_R = 2000$ MW; $B_1 = B_2 = 0.425$ p.u.MW/Hz; $R_1 = R_2 = R_3 = 2.4$ Hz/p.u.; $T_G = 0.08$ s; $T_T = 0.3$ s; $K_R = 0.3$; $T_R = 10$ s; $T_{GH} = 0.2$ s; $T_{RS} = 5$ s; $T_{RH} = 28.75$ s; $T_W = 1$ s; $X = 0.6$ s; $Y = 1$ s; $B = 0.05$; $C = 1$; $T_{CR} = 0.3$ s; $T_{FC} = 0.23$ s; $T_{CD} = 0.3$ s; $K_T = 0.6$; $K_H = 0.25$; $K_G = 0.15$; $K_{PS} = 120$ Hz/p.u.MW; $T_{PS} = 20$ s; $K_{DC} = 1$; $T_{DC} = 0.2$ s; $T_{12} = 0.0433$ p.u.; $a_{12} = -1$.

C. Three-area unequal reheat power system with GDB, GRC connected WT [25]

WT: $K_W = K_{PC} = 0.04$; $T_W = 4$ s; $K_{IG} = 1.494$; $K_1 = 1.25$; $T_1 = 0.6$ s; $K_2 = 1$; $T_2 = 0.041$ s; $K_3 = 1.4$; $T_3 = 1$ s; Power system: $P_{R1} = 2000$ MW; $P_{R2} = 4000$ MW; $P_{R3} = 8000$ MW; $B_1 = 0.3483$ p.u.MW/Hz; $B_2 = 0.3827$ p.u.MW/Hz; $B_3 = 0.3692$ p.u.MW/Hz; $R_1 = 3.0$ Hz/p.u.; $R_2 = 2.73$ Hz/p.u.; $R_3 = 2.82$ Hz/p.u.; $T_{G1} = 0.08$ s; $T_{G2} = 0.06$ s; $T_{G3} = 0.07$ s; $T_{T1} = 0.4$ s; $T_{T2} = 0.44$ s; $T_{T3} = 0.3$ s; $K_R = 0.5$; $T_R = 10$ s; $T_{12} = 0.2$ p.u.; $T_{23} = 0.12$ p.u.; $T_{31} = 0.25$ p.u.; $a_{12} = -P_{R1} = P_{R2} = -0.5$; $a_{23} = -P_{R2} = P_{R3} = -0.5$; $a_{13} = -P_{R1} = P_{R3} = -0.25$.

REFERENCES

- [1]. R. Shankar, S.R. Pradhan, K. Chatterjee, R. Mandal, "A comprehensive state of the art literature survey on LFC mechanism for power system", *Renewable and Sustainable Energy Reviews*. vol. 76, pp. 1185-1207, 2017
- [2]. Y.V. Hote, S. Jain, "PID controller design for load frequency control: Past, Present and future challenges", *IFAC-PapersOnLine*. vol. 51, no. 4, pp. 604-609, 2018
- [3]. D. Guha, P.K. Roy, S. Banerjee, "Application of backtracking search algorithm in load frequency control of multi-area interconnected power system", *Ain Shams Engineering Journal*. vol. 9, no. 2, pp. 257-276, 2018
- [4]. E.S. Ali, S.M. Abd-Elazim, "BFOA based design of PID controller for two area Load Frequency Control with nonlinearities", *International Journal of Electrical Power & Energy Systems*. vol. 51, pp. 224-231, 2013
- [5]. S.S. Dhillon, J.S. Lather, S. Marwaha, "Multi objective load frequency control using hybrid bacterial foraging and particle swarm optimized PI

- controller", *International Journal of Electrical Power & Energy Systems*. vol. 79, pp. 196-209, 2016
- [6]. G. Chen, X. Tan, Z. Zhang, Z. Sun, "Parameter optimization of pid sliding mode controller for hydraulic turbine regulating system based on IFABC algorithm", *Engineering Letters*. vol. 28, no. 1, pp. 168-179, 2020
- [7]. M.I. Mosaad, F. Salem, "LFC based adaptive PID controller using ANN and ANFIS techniques", *Journal of Electrical Systems and Information Technology*. vol. 1, no. 3, pp. 212-222, 2014
- [8]. S.A. Taher, M. Hajiakbari Fini, S. Falahati Aliabadi, "Fractional order PID controller design for LFC in electric power systems using imperialist competitive algorithm", *Ain Shams Engineering Journal*. vol. 5, no. 1, pp. 121-135, 2014
- [9]. J. Sharma, Y.V. Hote, R. Prasad, "Robust PID Load Frequency Controller Design with Specific Gain and Phase Margin for Multi-area Power Systems", *IFAC-PapersOnLine*. vol. 51, no. 4, pp. 627-632, 2018
- [10]. J. Yang, X. Sun, K. Liao, Z. He, L. Cai, "Model Predictive Control based Load Frequency Control for Power Systems with Wind Turbine Generators", *IET Renewable Power Generation*. vol. 13, no. 15, pp. 2871 - 2879, 2019
- [11]. B. Sonker, D. Kumar, P. Samuel, "Dual loop IMC structure for load frequency control issue of multi-area multi-sources power systems", *International Journal of Electrical Power & Energy Systems*. vol. 112, pp. 476-494, 2019
- [12]. Y. Mi, Y. Fu, D. Li, C. Wang, P.C. Loh, P. Wang, "The sliding mode load frequency control for hybrid power system based on disturbance observer", *International Journal of Electrical Power & Energy Systems*. vol. 74, pp. 446-452, 2016
- [13]. G. Chen, Z. Li, Z. Zhang, S. Li, "An Improved ACO Algorithm Optimized Fuzzy PID Controller for Load Frequency Control in Multi Area Interconnected Power Systems", *IEEE Access*. vol. 8, pp. 6429-6447, 2020
- [14]. R.K. Sahu, S. Panda, N.K. Yegireddy, "A novel hybrid DEPS optimized fuzzy PI/PID controller for load frequency control of multi-area interconnected power systems", *Journal of Process Control*. vol. 24, no. 10, pp. 1596-1608, 2014
- [15]. S. Mishra, A.K. Barisal, B.C. Babu, "Invasive weed optimization-based automatic generation control for multi-area power systems", *International Journal of Modelling & Simulation*. vol. 39, no. 3, pp. 190-202, 2019
- [16]. R.K. Sahu, S. Panda, S. Padhan, "A novel hybrid gravitational search and pattern search algorithm for load frequency control of nonlinear power system", *Applied Soft Computing*. vol. 29, pp. 310-327, 2015
- [17]. A. Fathy, A.M. Kassem, "Antlion optimizer-ANFIS load frequency control for multi-interconnected plants comprising photovoltaic and wind turbine", *ISA Transactions*. vol. 87, pp. 282-296, 2019
- [18]. A.N. Al-Rabadi, M.A. Barghash, "Fuzzy-PID control via genetic algorithm-based settings for the intelligent DC-to-DC step-down buck regulation", *Engineering Letters*. vol. 20, no. 2, pp. 176-195, 2012
- [19]. Z. Tian, X. Gao, D. Wang, "The application research of fuzzy control with self-tuning of scaling factor in the energy saving control system of pumping unit", *Engineering Letters*. vol. 24, no. 2, pp. 187-194, 2016
- [20]. Y. Arya, "AGC of two-area electric power systems using optimized fuzzy PID with filter plus double integral controller", *Journal of the Franklin Institute*. vol. 355, no. 11, pp. 4583-4617, 2018
- [21]. C. Li, H. Li, P. Kou, "Piecewise function based gravitational search algorithm and its application on parameter identification of AVR system", *Neurocomputing*. vol. 124, pp. 139-148, 2014
- [22]. R.K. Sahu, S. Panda, S. Padhan, "Optimal gravitational search algorithm for automatic generation control of interconnected power systems", *Ain Shams Engineering Journal*. vol. 5, no. 3, pp. 721-733, 2014
- [23]. M. Gheisarnejad, "An effective hybrid harmony search and cuckoo optimization algorithm based fuzzy PID controller for load frequency control", *Applied Soft Computing*. vol. 65, pp. 121-138, 2018
- [24]. R.K. Sahu, S. Panda, G.T. Chandra Sekhar, "A novel hybrid PSO-PS optimized fuzzy PI controller for AGC in multi area interconnected power systems", *International Journal of Electrical Power & Energy Systems*. vol. 64, pp. 880-893, 2015
- [25]. F. Li, W. Yu, Z. Zhang, "Load Frequency Control for Multi-area Power System with Wind Power Generation", *Water Resources and Power*. vol. 36, no. 1, pp. 195-199, 2018